PCCP

How does multi-reference computation change the catalysis chemistry? DFT and CASPT2 studies of the Cu-catalysed coupling reactions between aryl iodides and β-diketones

SCHOLARONE™
Manuscripts

1

How does multi-reference computation change the catalysis

2

chemistry? DFT and CASPT2 studies of the Cu-catalysed

3

coupling reactions between aryl iodides and β-diketones

4   Nan He[1], Naoki Nakatani[1,*], Masahiko Hada[1]

5   *[1] Department of Chemistry, Faculty of Science, Tokyo Metropolitan University,*

6   *1-1 Minami-Osawa, Hachioji, Tokyo, 192-0397, Japan*

7

8   E-mail: naokin@tmu.ac.jp

9

10   **Abstract:** The molecular mechanism of a Cu-catalysed coupling reaction was theoretically studied

11   using density functional theory (DFT) and the complete active space self-consistent field method

12   followed by the second-order perturbation theory (CASSCF/CASPT2) to investigate the effects of the

13   strong electron correlation of the Cu centre on the reaction profile. Both DFT and CASSCF/CASPT2

14   calculations showed that the catalytic cycle proceeds via an oxidative addition (OA) reaction, followed

15   by a reductive elimination (RE) reaction, where OA is the rate-determining step. Although the DFT-

16   calculated activation energies of the OA and RE steps are highly dependent on the choice of functionals,

17   the CASSCF/CASPT2 results are less affected by the choice of DFT-optimised geometries. Therefore,

18   with a careful assessment based on the CASSCF/CASPT2 single-point energy evaluation, an optimal

19   choice of the DFT geometry is of good qualitative use for energetics at the CASPT2 level of theory.

20   Based on the changes in the electron populations of the 3d orbitals during the OA and RE steps, the

21   characteristic features of the DFT-calculated electronic structure were qualitatively consistent with those

22   calculated using the CASSCF method. Further electronic structure analysis by the natural orbital

23   occupancy of the CASSCF wavefunction showed that the ground state is almost single-reference in this

24   system and the strong electron correlation effect of the Cu centre can be dealt with MP2 or CCSD

25   method, too. However, the slightly smaller occupation numbers of $3d\pi$ orbital in the course of reactions,

26   suggested that the electron correlation effect of the Cu(III) centre appears through the interaction

27   between the $3d\pi$ orbital and the C-I antibonding σ^* orbital in the OA step, and between the $3d\pi$ orbital

28   and the Cu-C antibonding σ^* orbital in the RE step.

29

32

33

34

1. Introduction

Computational chemistry based on quantum mechanics has grown rapidly with the development of density functional theory (DFT)[1-4] since the 1990s, which has enabled the characterisation of reaction intermediates and transition states to reveal the microscopic mechanisms of various chemical reactions. Despite its success in computing organic compounds, the DFT method frequently suffers from computational accuracy issues for transition-metal complexes because of the complicated electronic structure consisting of d electrons.[5] Various density functionals have been proposed to address this issue. However, a universal functional has not yet been proposed, and another arbitrariness problem arises in the choice of functionals. This functional dependency worsens, especially in 3d transition metals such as Fe, Ni, and Cu, owing to the strong electron correlation effect of 3d electrons.[6-8]

One approach to capturing the strong electron correlation effect is the multireference wavefunction method, in which the complete active space self-consistent field (CASSCF)[9, 10] is followed by the second-order perturbation theory (CASPT2).[11-13] However, applications of such multireference methods to medium-sized or larger molecules are limited because the multireference method is computationally very expensive. Nonetheless, CASSCF/CASPT2 has garnered renewed attention as a potential application in quantum computers, with promising implications for the future development of electronic state theory and quantum computers.[14-18] In this study, we focused on a Cu-catalysed cross-coupling reaction as an example of a simple catalytic reaction involving a 3d transition metal complex. We employed both DFT and CASSCF/CASPT2 methods to compare the geometry, electronic structure, and reaction mechanism, and discussed what kind of computational strategy would work for the Cu-catalyzed coupling reaction. The CASSCF/CASPT2 method is used to investigate the reaction mechanism. It should be noted that the maintaining the same active space for each complex during the reaction is challenging.[19-22] Therefore, we selectively chose important orbital that contribute significantly to the reaction within the active space, ensuring consistency in the active space for each complex.

Coupling reactions catalysed by 3d transition metal complexes have become an active research field owing to their simple raw materials and wide applications.[23-26] In particular, some good Cu complex catalysts have been reported to replace toxic and/or expensive metal catalysts such as Pd or Ni complexes.[27, 28] For instance, Ullmann reactions can be utilised to form C-C bonds,[29, 30] C-O bonds,[31-35] and C-N bonds[36, 37] between aryl compounds from aryl halides and arenes, phenols, and amines catalysed by copper catalysts, which have become increasingly popular owing to their high catalytic activity, low toxicity, and good cost-performance.[38] On the other hand, Cu-catalysed coupling reactions also face many challenges due to high metal loading, harsh experimental conditions, and a narrow reaction scope. This has led many theoretical chemists to study the reaction mechanism to improve catalytic activity, selectivity, and reaction scope. Mechanistic studies on Ullmann reactions have been conducted since the 1960s; however, the proposed mechanisms vary depending on the specific experimental conditions and the nature of the reactants and catalysts.[39-43] In Ullmann reactions, the Cu^0, Cu^I, or Cu^{II} complex is often considered a catalytically active species to initiate the reaction.[44-46] Furthermore, the Cu^{III} species can

2

1   be formed as unstable intermediates by either two-electron transfer oxidation or single-electron transfer

2   reactions from the Cu^I/Cu^{II} intermediates. These Cu^{III} species possess strong oxidising abilities that

3   promote coupling reactions with nucleophiles, followed by RE reactions.[47-49]

4   Recently, Lei et al. reported a new Cu-catalysed coupling reaction in which β-diketones act as either

5   a reactant or a ligand (Scheme 1(a)),[50] in which the disproportionation of the Cu(I) complex easily leads

6   to the formation of Cu^{II} and Cu^0 complexes under experimental conditions. Based on DFT calculations,

7   they suggested that a small amount of the Cu(I) complex formed under equilibrium conditions works as

8   a catalytically active species in the oxidative addition-reductive elimination (OA-RE) pathway. In

9   contrast, Jones suggested that the Cu^{II} complex plays a crucial role in the catalytic cycle via the single-

10   electron transfer (SET) mechanism with a similar ligand, which was also discussed based on DFT

11   calculations.[41] Therefore, it is worthwhile to revisit the reaction mechanism based on the

12   CASSCF/CASPT2 method, which can correctly incorporate the strong electron correlation effect from

13   3d transition metal elements, at least qualitatively.

14   For Cu complexes, Pierloot and co-workers conducted a CASSCF/CASPT2 study on the metal-

15   ligand bonds in various Cu(II) complexes to demonstrate the significance of the electron correlation

16   effects in the spin states and excitation energies.[51-54] They compared the DFT and CASSCF/CASPT2

17   results for an O_2-binding reaction to the dicopper complex and found that the results obtained from these

18   methods differ significantly.[52] They also performed the CASSCF/CASPT2 calculations on the electronic

19   spectra of blue copper proteins and concluded that the CASSCF/CASPT2 reproduced the spectra to

20   provide valuable insights.[53] Additionally, the Vlaisavljevich and co-workers employed the

21   CASPT2/CASSCF method to investigate the geometry and electronic structure of Cu corroles with a

22   small active space (4e,5o), which is in good agreement with experimental results.[55] The Ferrão and co-

23   workers discovered that the $Cu(AcAc)_3$ complex exhibited multiconfigurational characteristics by

24   CASSCF/CASPT2 method.[56] Thus, the CASSCF/CASPT2 method is a useful tool for theoretical

25   investigation on Cu complexes.

26   In this study, we considered four possible reaction pathways: oxidative addition-reductive

27   elimination (OA-RE), iodine atom transfer (IAT), single-electron transfer (SET), and σ-bond metathesis

28   (Scheme 1). Herein, we theoretically investigated the active species and reaction mechanism based on

29   DFT and CASSCF/CASPT2 methods to reveal the role of electron correlation effects in Cu-catalysed

30   coupling reactions.

31

(a) Reaction model
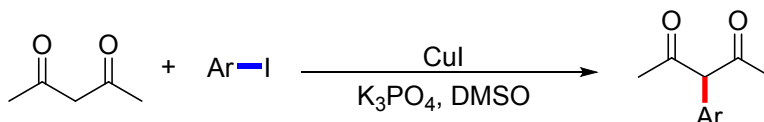
(b) Motivation
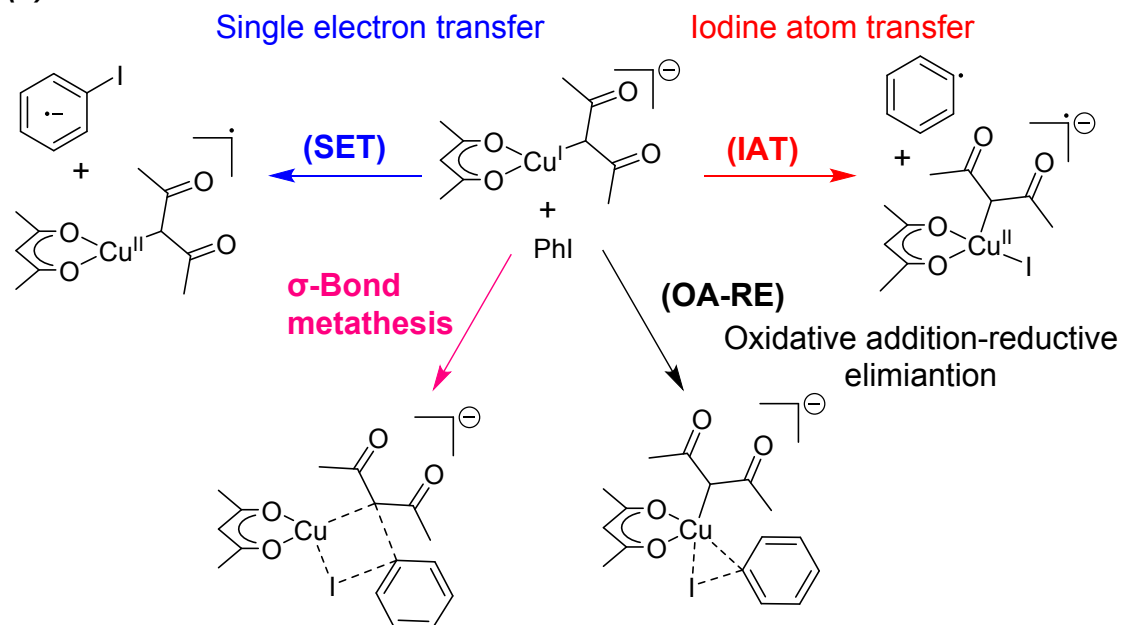
1
2   **Scheme 1.** The reaction of coupling reaction between aryl iodides and β-diketones.
3

2. Computational details

5   All density functional theory (DFT) calculations were performed using the Gaussian 16 program

6   (Revision B.01).[57] Several hybrid GGA and meta-GGA functionals, B3LYP-D3, ω-B97XD, PBE0,

7   TPSS, and MN15 were examined to investigate their functional dependency on the reaction mechanism.

8   We employed Stuttgart/Dresden valence basis sets for the Cu and I atoms, where 10 core electrons of

9   Cu and 46 core electrons of I were replaced by effective core potentials (ECP), ECP10MDF, and

10   ECP46MWB, respectively,[58, 59] For the other atoms, we employed 6-31G(d) basis sets for geometry

11   optimisation, and 6-311+G(d, p) basis sets for energy evaluation. The solvent effect of dimethyl

12   sulfoxide (DMSO) was considered based on the polarised continuum model (PCM)[60] with a dielectric

13   constant of 46.826. For each optimised geometry, vibrational mode analysis was carried out at the same

14   computation level to ensure that the reactant, intermediate, or product structure had no imaginary

15   frequencies or that the transition state had only one imaginary frequency. Intrinsic reaction coordinate

16   (IRC) calculations were performed for each transition-state structure to obtain the minimum energy path

17   (MEP) for the elementary reaction.

18   To perform an energy evaluation by incorporating the strong electron correlation effect of 3d

19   transition metals, we also carried out CASSCF/CASPT2 calculations using the Molcas 8.4 program

20   package.[61, 62] The same basis sets as those used in the DFT calculations were employed for the I and Cu

21   atoms, while cc-pVTZ basis sets were employed for the other atoms. The solvent effect of DMSO was

1 considered the same as that observed in the DFT calculations. We included 12 electrons within 12
2 orbitals as the active space for the OA and RE reactions, in which five 3d and five 4d orbitals of Cu and
3 σ and σ* orbitals describing bond cleavage/formation of each elementary reaction. We also employed
4 the imaginary level shift of 0.1 a.u. to successfully remove intruder states in CASPT2 calculations.[63]
5 Choice of the active space and its assessment were further discussed in the Supporting Information.

6   In addition, we performed the MP2 and the CCSD calculations based on the ω-B97XD-optimised
7 geometry, using Gaussian 16 program, to compare the electronic energy profile with those calculated
8 by the DFT and the CASPT2 methods. The same basis sets as the CASPT2 calculation and the solvation
9 effect of DMSO were considered in the MP2 and the CCSD calculations.

10
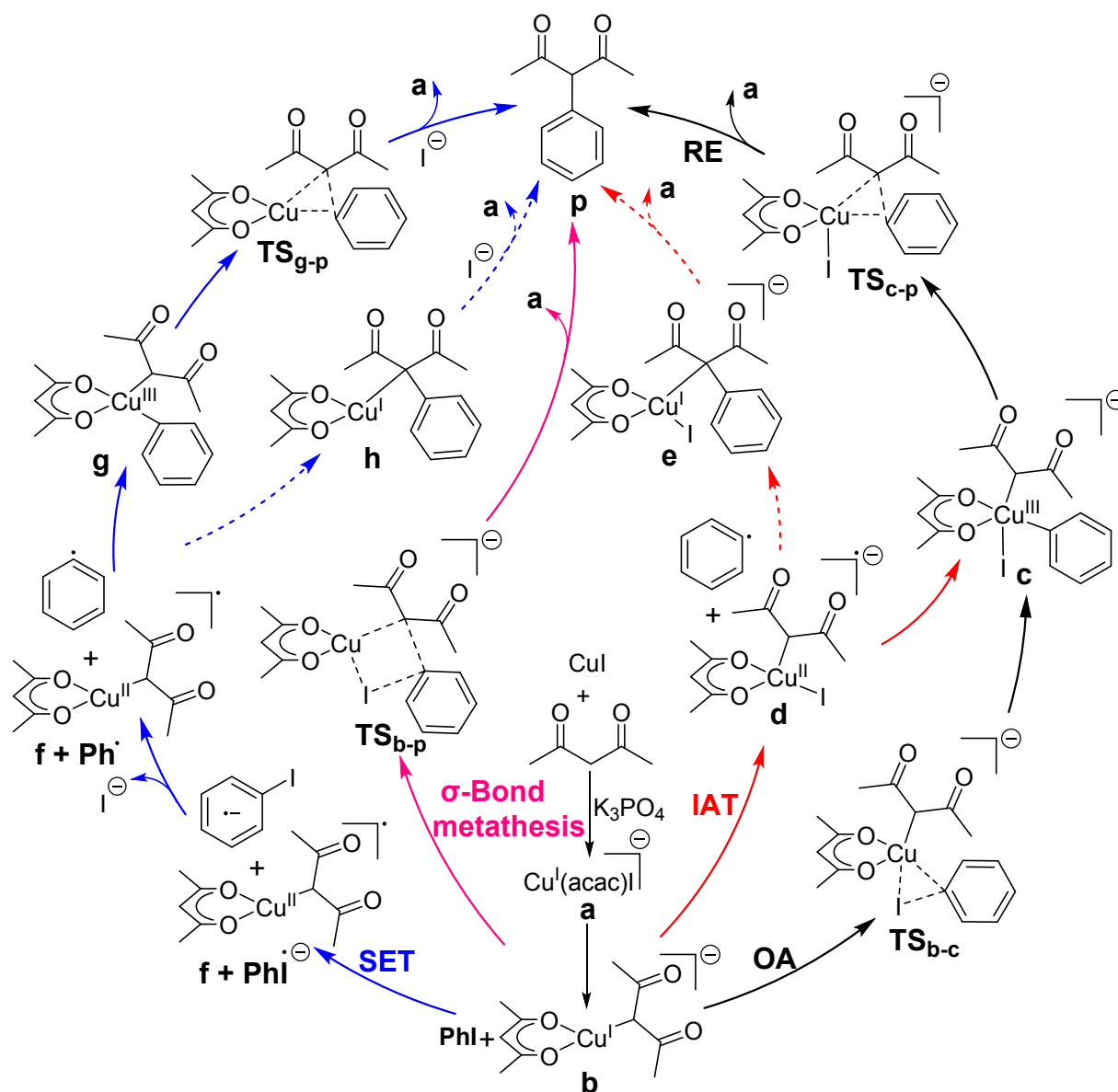
Scheme 2. The different reaction pathways proposed from the previous works on the Cu-catalyzed coupling reaction between aryl iodides and β-diketones. (a) The OA-RE mechanism, (b) IAT mechanism, (c) σ-bond metathesis mechanism, and (d) SET mechanism.

3. Results and Discussion

3.1 Mechanistic aspects of Cu-catalysed cross-coupling reaction between aryl iodides and β-diketones.

First, we theoretically investigated the possible reaction pathways of the Cu-catalysed cross-coupling reaction between aryl iodides and diketones based on ω-B97XD calculations. Four different mechanisms proposed in the previous studies were summarized in Scheme 2; OA-RE, IAT, σ-bond metathesis, and SET mechanisms.

3.1.1 OA-RE pathway

In the OA-RE mechanism, the catalytic reaction consists of two elementary steps, namely, the oxidative addition (OA) reaction and the reductive elimination (RE) reaction. Before the OA step, Cu(I)-diketonate complex **a** was formed by the reaction of the pre-catalyst CuI and β-diketone with the help of a base (K$_3$PO$_4$), and then complex **a** was converted into the active catalyst [Cu^I(η^2-β-diketone)(β-diketonate)]$^-$ complex **b**. Initially, the **PhI** interacts with the **b** to form the precursory complex **PhI...b**. In the OA step, the active catalyst **b** reacts with the reactant **PhI** to form Cu(III) intermediate **c** via a Cu-C-I three-membered ring transition state **TS$_{b-c}$**. In Figure 1, the C1-I2 bond length increases from 2.36 Å in **TS$_{b-c}$** to 3.21 Å in **c**, indicating the C1-I2 bond breaking. The Cu3-C1 and Cu3-I2 distances decrease from 2.09 Å and 2.62 Å in **TS$_{b-c}$** to 1.91 Å and 2.63 Å in **c**, respectively, indicating the formation of Cu3-C1 and Cu3-I2 bonds. Note that the Cu3-O4 distance of 2.24 Å is significantly larger than the Cu3-O5 distance of 1.94 Å in complex **c**, suggesting that the Cu3-O4 dative bond is weaker than the Cu3-O5 dative bond. Hence, the Cu(III) intermediate **c** adopts a four-coordinate square-planar geometry, which is assigned as the d^8-complex. The activation free energy ($\Delta G^{\ddagger}$) of the OA step was computed to be 25.0 kcal/mol, which provided the lowest activation barrier amongst the four considered mechanisms (Figure 1). The reaction is followed by the RE step on Cu(III) complex **c** to form the final product **p** via the transition state **TS$_{c-p}$** for C1-C6 bond formation and the regeneration of an active complex **a**. The Cu3-C1 and Cu3-C6 distances increase from 1.91 Å and 2.06 Å in **c** to 1.92 Å and 2.08 Å in **TS$_{c-p}$**, respectively, indicating the breaking of Cu3-C1 and Cu3-C6 bonds. And the distance of C1-C6 decreases from 2.64 Å in **c** to 2.08 Å in **TS$_{c-p}$**, which suggests that the C1-C6 bond is forming. $\Delta G^{\ddagger}$ in the RE step was computed to be 15.5 kcal/mol, showing that the OA step is a rate-determining step (RDS) in the OA-RE pathway. Note that the activation barrier from **c** to **TS$_{c-p}$** was estimated to be slightly negative (-0.8 kcal/mol). This was because the free energy correction based on harmonic oscillators failed in case of a shallow transition state. Therefore, it is concluded that the RE step could occur with almost no barrier on the ω-B97XD-computed free energy profile. The Gibbs free energy profile of the OA-RE pathway in the triplet spin state was also investigated (Figure S1). However, the triplet spin state always has a higher energy than the singlet spin state along the reaction coordinates. This indicates that there is no intersystem crossing point (ISCP) between the singlet and triplet spin states. Thus, the contribution of the triplet spin state to the OA-RE pathway was ruled out. Thus, the OA-RE pathway is expected to be the most reliable mechanism at the DFT level. We also examined several DFT functionals to compute

1   the overall activation barrier and concluded that the DFT results were qualitatively the same for these

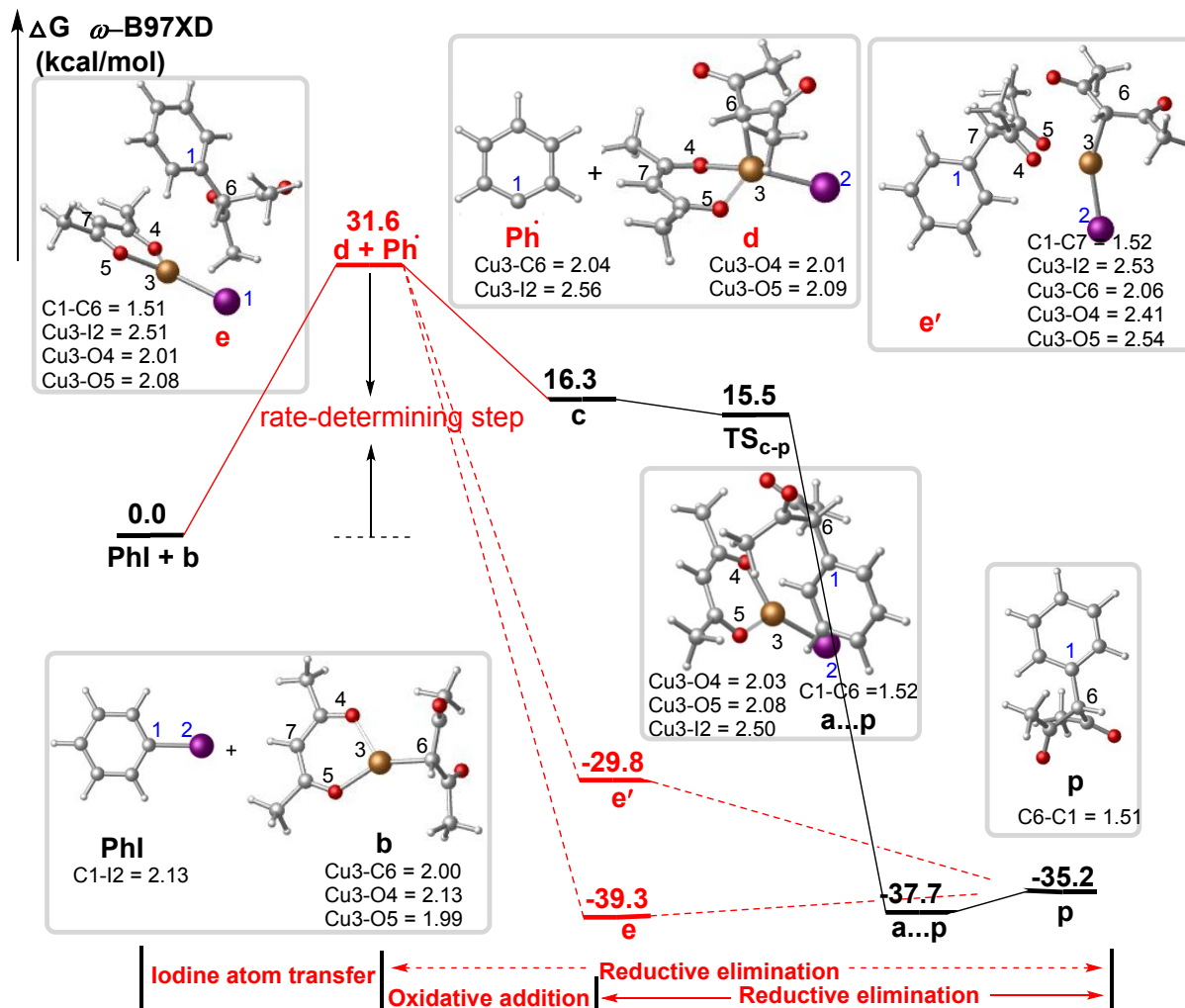2   functionals (see the discussion in Section 3.3).
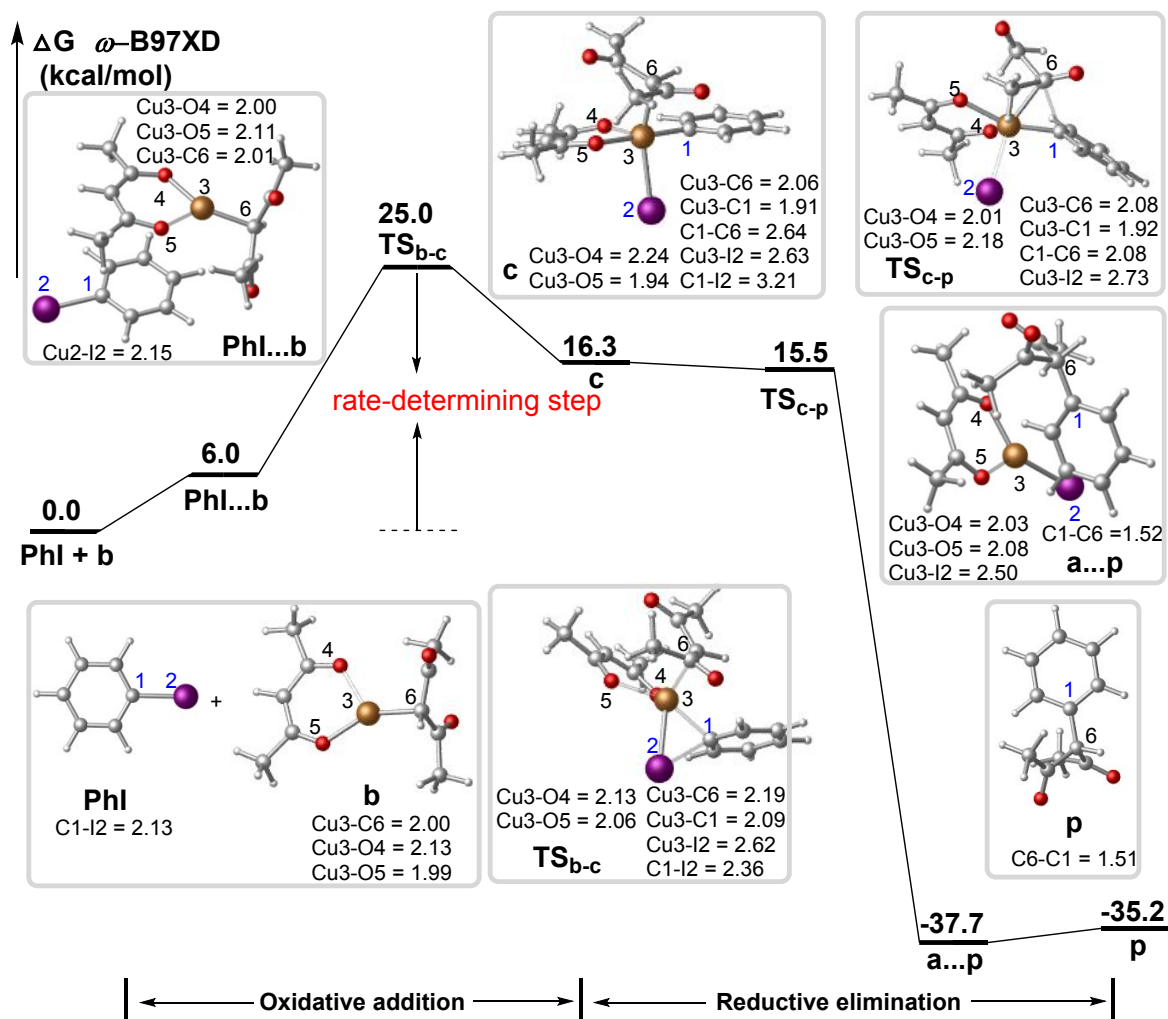
3

4   **Figure 1.** The Gibbs free energy profiles for OA-RE pathway (Distance in Å; small gray ball-hydrogen,

5   gray-carbon, red-oxygen, yellow-copper, and purple-iodine).

6

3.1.2 IAT pathway

8   In the IAT mechanism, iodine atom transfer occurs from a reactant **PhI** to the active catalyst **b** to

9   afford a four-coordinated tetrahedral complex [Cu^{II}I(η^2-β-diketone)(β-diketonate)]$^-$ (**d**) and phenyl

10   radical, which was computed to be endothermic by 31.6 kcal/mol and no transition state was found in

11   this process, i.e., potential energy monotonically increases along the iodine atom transfer (Figure S2).

12   There are three possible pathways through which the phenyl radical attacks the Cu^{II} complex **d** (see

13   Figure 2): (1) to the Cu^{II} centre to afford the Cu^{III} complex **c** which is the same intermediate in the OA-

14   RE pathway, followed by the RE step; (2) to the C6 of the β-diketonyl to form a Cu^{I} intermediate **e**; and

15   (3) to the C7 of the β-diketonate to form a Cu^{I} intermediate **e'**. These radical coupling reactions occur

16   without activation barriers. Intermediates **e** and **e'** were computed to be more stable than the complex **b**

17   by 39.3 and 29.8 kcal/mol, respectively. From intermediates **e** and **e'**, the product can be easily

1   dissociated to regenerate catalyst **b** and its isomer. The Gibbs free energy profile of the IAT pathway in

2   the triplet spin state was also investigated (Figure S3). However, the triplet spin state always has a higher

3   energy than the singlet spin state along the reaction coordinates. This indicates that IAT pathway was

4   highly unstable so that the reaction would not occur in the triplet spin state.

6   **Figure 2.** The Gibbs free energy profiles for IAT pathway (Distance in Å; small gray ball-hydrogen,

7   gray-carbon, red-oxygen, yellow-copper, and purple-iodine).

8

9   **3.1.3 SET pathway**

10   In the SET mechanism, the reaction is initiated by electron transfer from the Cu^{I} centre to the **PhI**

11   molecule to form the Cu^{II} active species **f** and the radical anion of **PhI**. According to a previous work

12   by Houk and Buchwald, the **PhI** radical anion easily fragments to form a phenyl radical and an iodide

13   anion.[41] Similar to the IAT mechanism, there are also three possible pathways depending on where the

14   phenyl radical attacks. In the case that the phenyl radical attacks the Cu^{II} center, a Cu^{III} phenyl complex

15   **g** is formed, which was computed to be somewhat less stable than the complex **b** by 12.1 kcal/mol (see

16   Figure 3). The Cu^{III} phenyl complex **g** is a four-coordinate square-planar d^{8}-complex. The reaction was

17   followed by an RE step (see Section 3.1.1). When the phenyl radical attacks the C6 of the β-diketonyl

8

1   ligand, it generates Cu^I complex **h**, which was found to be more stable than complex **b** by 26.0 kcal/mol.

2   When the phenyl radical attacks C7 of the β-diketonyl ligand, the Cu^I complex **h'** is generated, which

3   was computed to be more stable than complex **b** by 22.8 kcal/mol. From the generated intermediates **h**

4   and **h'**, the product can be easily dissociated, thereby regenerating catalyst **b** and its isomer. The Gibbs

5   free energy profile of the SET pathway was examined in the triplet spin state (Figure S4). But it was

6   found that triplet state always has a higher energy than single state along the reaction coordinates. This

7   indicates that the SET pathway was highly unstable and would not occur in the triplet spin state.

8
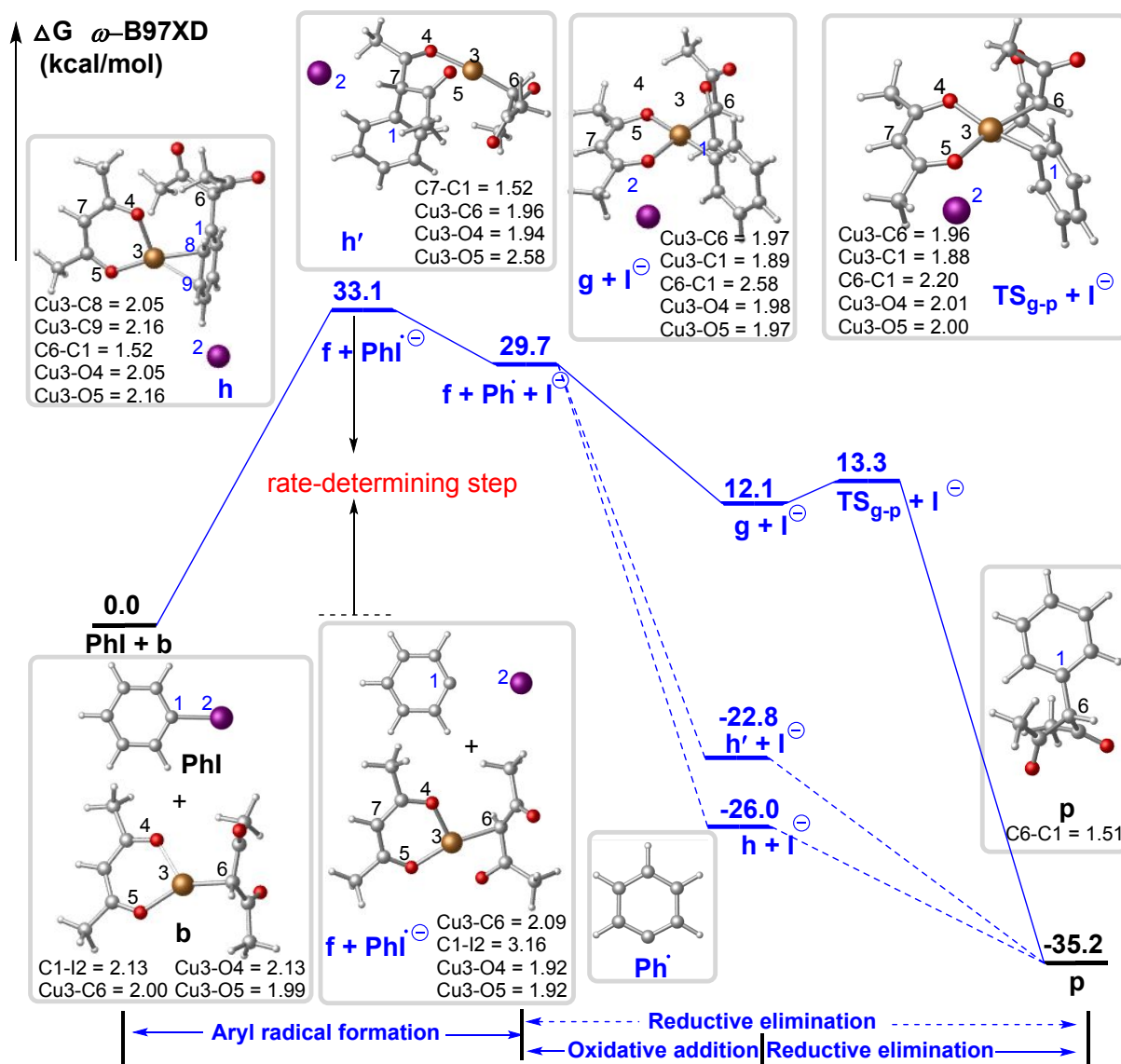
9

10   **Figure 3.** The Gibbs free energy profiles for SET pathway (Distance in Å; small gray ball-hydrogen,

11   gray-carbon, red-oxygen, yellow-copper, and purple-iodine).

12

13   **3.1.4 σ-bond metathesis pathway**

14   In the σ-bond metathesis mechanism, the reaction should follow a concerted S$_{N2}$ pathway through

15   the Cu-C-C-I four-membered ring transition state **TS$_{b-p}$**, leading to the formation of the final product

1   (see Scheme 2). However, we were unable to locate $TS_{b\text{-}p}$, most likely because of the considerable steric

2   hindrance of the β-diketone in $TS_{b\text{-}p}$, which rendered the four-membered ring unstable. Consequently,

3   the σ-bond metathesis pathway does not exist; therefore, the Gibbs free energy of $TS_{b\text{-}p}$ is not provided.

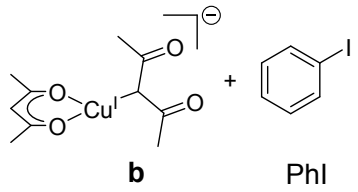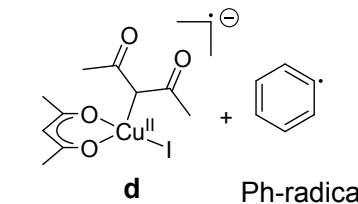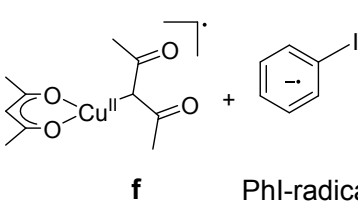4   **3.1.5 Summary of the DFT calculated pathways.**

5   Next, we summarise the DFT-calculated results. In the OA-RE pathway, the rate-determining step

6   was estimated to be the OA step with an activation barrier of 25.0 kcal/mol in Gibbs free energy. In the

7   IAT pathway, the formation of $[Cu^{II}I(\eta2\text{-}\beta\text{-diketone})(\beta\text{-diketonate})]^{-}$ complex **d** and the phenyl radical

8   was computed to be a highly endergonic process with an energy barrier of at least 31.6 kcal/mol.

9   Similarly, in the SET mechanism, the formation of the $[Cu^{II}(\eta2\text{-}\beta\text{-diketone})(\beta\text{-diketonate})]$ active

10   species **f** and the radical anion of PhI were also highly endergonic by 33.1 kcal/mol. Comparing these

11   three pathways, we concluded that the OA-RE pathway was the most favourable under the experimental

12   conditions, which is consistent with the previous work by Lei,[50] whereas the occurrence of IAT and SET

13   pathways is less likely from the DFT results.

14

15   **3.2 CASSCF/CASPT2 analysis on the precursory complexes.**

16   To confirm the reliability of the DFT results, the energies and electronic structures of the precursor

17   complexes were evaluated at the CASSCF/CASPT2 level of theory for the OA-RE (**b**), IAT (**d**), and

18   SET (**f**) pathways. The active orbitals and their occupation numbers for complexes **d**, **b**, and **f** are shown

19   in Figure S5. The electronic energies of the precursory complexes calculated using the ω-B97XD

20   functional and CASPT2 methods are summarised in Table 1. Here, we considered electronic energy (i.e.

21   not Gibbs free energy) in either ω-B97XD or CASPT2 calculation. As discussed in the above

22   subsections, the ω-B97XD results suggested that the precursory complex **d** in the OA-RE pathway was

23   the most stable; complex **d** in the IAT pathway and complex **f** in the SET pathway were computed to be

24   higher in electronic energy by 31.8 and 35.5 kcal/mol with complex **b**. These results indicate that the

25   formation of the radical pair is highly endothermic. The CASPT2 results showed a trend similar to the

26   ω-B97XD results; complexes **d** and **f** were computed to be higher in energy by 45.3 and 57.1 kcal/mol

27   with complex **b**. Therefore, both the IAT and SET pathways were safely excluded from the catalytic

28   cycle and we focused on the OA-RE pathway.

29

30

1   **Table 1.** The electronic energy of precursory complex in IAT, OA-RE and SET mechanisms.

|	Complexes		ΔE ω-B97XD	ΔE CASPT2//ω-B97XD
OA RE	**b**	**PhI**	0.0 kcal/mol	0.0 kcal/mol
IAT	**d**	Ph-radical	31.8 kcal/mol	45.3 kcal/mol
SET	**f**	PhI-radical	35.5 kcal/mol	57.1 kcal/mol

2
3

3.3 DFT functional dependency in OA-RE pathway.

5   In this subsection, we discuss the functional dependence of the OA-RE pathway on DFT. We
6 examined several functionals, B3LYP-D3, ω-B97XD, PBE0, TPSS, and MN15 to perform geometry
7 optimisation, and the single-point energies were evaluated using the CASPT2 method based on the DFT-
8 optimised geometries. In the OA step, we considered 12 electrons in 12 orbitals as active spaces for
9 complexes **PhI...b**, **TS$_{b-c}$**, and **c**, which included five 3d orbitals and corresponding five unoccupied d
10 orbitals, to incorporate the "double-shell" effect in the Cu^0 centre. Additionally, one C-C/C-I σ bond
11 orbital (or Cu 3p orbital) and its corresponding unoccupied orbital was considered (see Figure S6 in
12 detail). Complex **PhI...b** is a precursory complex where complex **b** weakly interacts with the **PhI**. We
13 optimised the geometry of **PhI...b** and its electronic energy was taken as the reference (energy zero) in
14 the OA step. In the RE step, we also considered 12 electrons in 12 orbitals as active spaces for complexes
15 **c**, **TS$_{c-p}$**, and **i**, which included five 3d orbitals and the corresponding five unoccupied d orbitals.
16 Additionally, we also added the Cu-C σ bond orbital (or Cu 3p orbital) and its corresponding unoccupied
17 orbital into active space (see Figure S7 in detail). Complex **a...p** is a product complex, in which product
18 **p** is weakly bound to complex **a**. We used complex **c** as the reference (energy zero) in the RE step.

19   The activation barriers for the OA and RE steps were calculated using the DFT and CASPT2
20 methods in electronic energy ($\Delta E^{\ddagger}$), as summarised in Figure 4. In the OA step, the activation barriers
21 calculated using the B3LYP-D3, ω-B97XD, TPSS, PBE0, and MN15 functionals were 13.3, 16.5, 10.5,
22 14.2 and 21.4 kcal/mol, respectively. From the single-point energy evaluations using the CASPT2
23 method based on the DFT-optimised geometries, these were corrected to 8.8, 8.6, 7.8, 6.1 and 8.5

1   kcal/mol, respectively. Interestingly, although the DFT-calculated activation barriers strongly depend

2   on the choice of functional (at most a 10.9 kcal/mol variation in energy), the CASPT2 results were less

3   affected by the choice of functional for geometry optimisation. This implies that the electronic energy

4   is highly dependent on the DFT functionals, whereas the optimised geometry is not. In the RE step, we

5   found the same trend that we found in the OA step: the DFT-calculated activation barriers were 6.7, 1.3,

6   9.1, and 4.2 kcal/mol for B3LYP-D3, ω-B97XD, TPSS, and PBE0 functionals, respectively, and those

7   calculated by the CASPT2 method were 6.0, 5.3, 7.9, and 4.8 kcal/mol, respectively. Note that the

8   transition state structure was not found with MN15 functional in the RE step (see Figure S9). We also

9   compared the CASPT2 energies of complex **c** among DFT-optimised geometries. As a result, the ω-

10   B97XD-optimized geometry gave the lowest CASPT2 energy, and the others were computed to be

11   higher in energy by 1.9, 3.4, 1.0 and 0.5 kcal/mol for B3LYP-D3, TPSS, PBE0, and MN15 respectively.

12   Interestingly, the ω-B97XD-optimised geometry showed a shorter C1-C6 distance (2.64 Å) in complex

13   **c** than that in the other complexes, indicating that it is advantageous to proceed with the RE reaction

14   (see Figure S10). This is because the energy barrier in the RE step calculated using the ω-B97XD

15   functional (1.3 kcal/mol) is the lowest among these DFT functionals. It should be noted that the ω-

16   B97XD functional is not always the optimal choice for other systems.[20] Thus, a careful assessment using

17   the CASSCF/CASPT2 single-point energy evaluation should always be carried out.
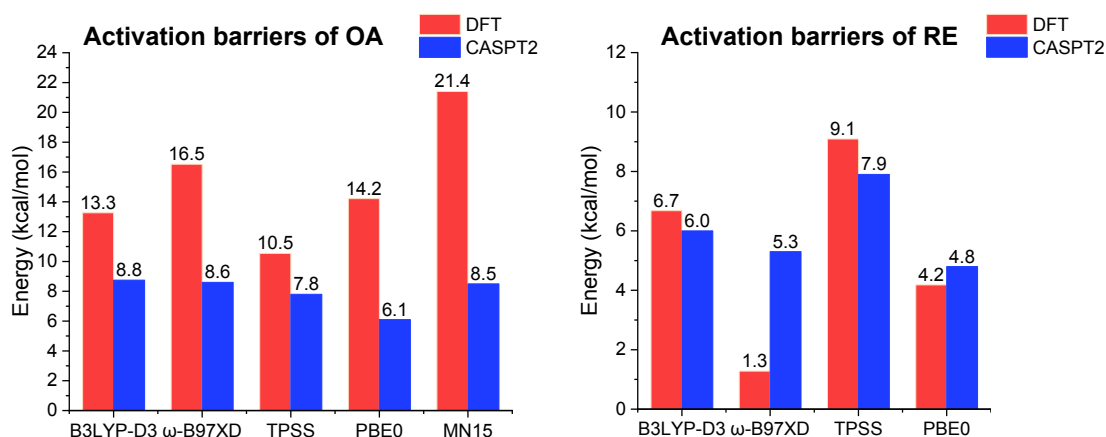
19   **Figure 4.** The activation barriers of OA and RE steps calculated by DFT and CASPT2 (Unit: kcal/mol).

20

21   **3.4 CASPT2 energy profile along the DFT-optimized geometry**

22   We also analysed the CASPT2-calculated activation energies based on the DFT-optimised

23   geometry. First, we defined the approximate activation energy of the CASPT2 method as the difference

24   between the single-point CASPT2 energies at the DFT-optimised geometries of complex **c** and $\mathbf{TS_{c\text{-}p}}$

25   ($\Delta E_{\text{CASPT2//DFT}}$). As described in Scheme 3, in case where positions of the stationary point and the

26   transition state are consistent between the DFT-optimised geometry and the real geometry (here we

27   assumed the CASPT2-optimised one), the CASPT2 activation energy can be accurately evaluated by

28   using the DFT-optimised geometry (Scheme 3(a)). On the other hand, in case where the positions are

29   different from each other, the CASPT2 activation energy can be underestimated based on the DFT-

1   optimised geometry (Scheme 3(b)).

2   According to our assumption from Scheme 3, we compared the $\Delta E_{\text{CASPT2//DFT}}$ of the OA and RE

3   steps employing several DFT funcitonals as summarized in Figure 4. From the single-point CASPT2

4   energies of complex **c**, ω-B97XD, PBE0, and MN15 functionals gave the lower energies than the other

5   functionals as discussed in the above subsection. Amongst them, the ω-B97XD functional gave the

6   higher $\Delta E_{\text{CASPT2//DFT}}$ value of 8.6 kcal/mol or 5.3 kcal/mol than the others either for the OA step or the

7   RE step, respectively. These discussions were also elucidated in the section 3.5.1 later on. Although the

8   TPSS functional gave the highest $\Delta E_{\text{CASPT2//DFT}}$ value of 7.9 kcal/mol in the RE step, it also gave the

9   highest single-point CASPT2 energy (i.e. 3.4 kcal/mol higher than the ω-B97XD-optimised geometry)

10   of complex **c**. Thus, we conclude that the ω-B97XD functional is better than the other functionals, at

11   least in the optimised geometry, and we employed the ω-B97XD-optimized geometry in all the

12   CASSCF/CASPT2 calculations, hereafter.

13
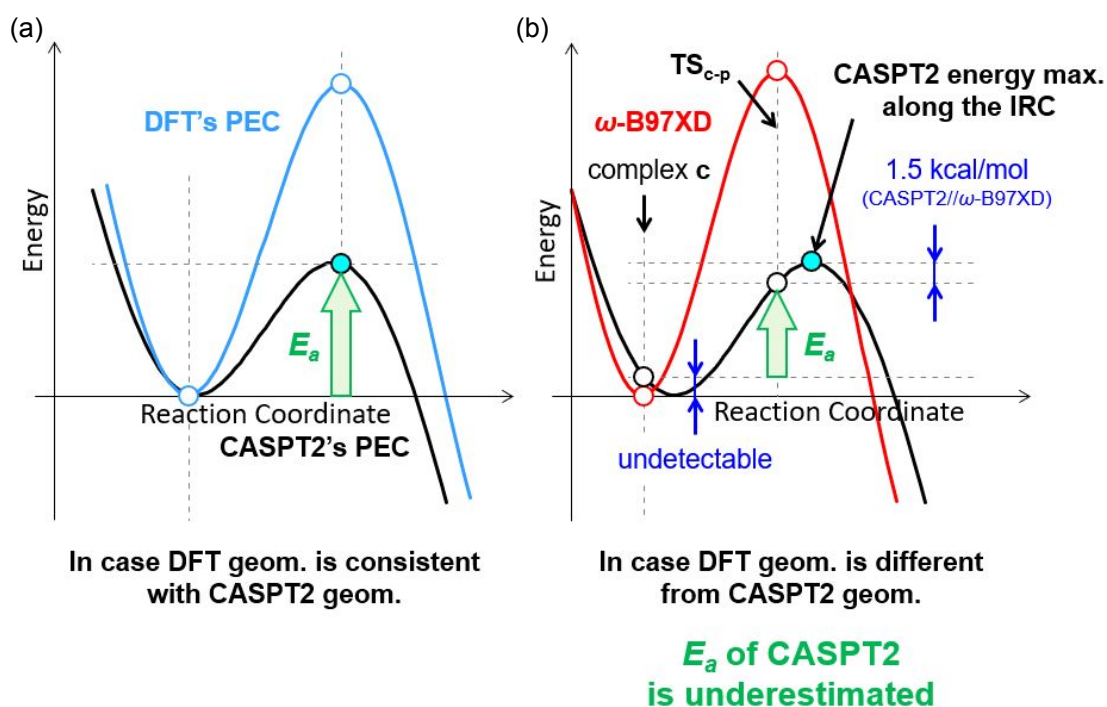
14
15   **Scheme 3.** Schematic explanation how to evaluate reliability of the DFT-optimised geometry for the

16   CASPT2 singlet point calculation. (a) A case where DFT and CASPT2 geometries are consistent with

17   each other. (b) A case where DFT and CASPT2 geometries are different from each other. In ω-B97XD-

18   optimised geometry, for instance, the energy error at **TS$_{\text{c-p}}$** was estimated to be 1.5 kcal/mol from the

19   IRC calculation as discussed in 3.5.2.

20

21   Finally, we summarised the electronic energy profile calculated using MP2, CCSD, and CASPT2

22   methods along the reaction coordinates obtained from the DFT-optimised geometry with ω-B97XD

23   functional (denoted as MP2//ω-B97XD, CCSD//ω-B97XD, and CASPT2//ω-B97XD, respectively). In

24   comparison with these electronic energy profiles, ω-B97XD, MP2, CCSD, and CASPT2 results

1   exhibited qualitatively the same trends (see Figure 5). Notably, the OA step was consistently identified

2   as the rate-determining step in all these calculations, though the MP2- and the CASPT2-calculated

3   activation barriers of 8.7 kcal/mol and 8.6 kcal/mol, respectively, were almost half of those 16.5 and

4   14.6 kcal/mol calculated by ω-B97XD functional and CCSD method, respectively. The MP2-calculated

5   reaction energy of 6.6 kcal/mol to form complex **c** was somewhat larger than the others, while all of

6   these gave quantitatively the same activation barriers in the RE step. Though we could not conclude

7   which method provided the most accurate results, we concluded that all these methods were reliable in

8   this system, at least qualitative manner. Since we are interested in the strong electron correlation effect

9   from Cu center, we focused on the DFT and the CASPT2 results, in the latter subsections.

10
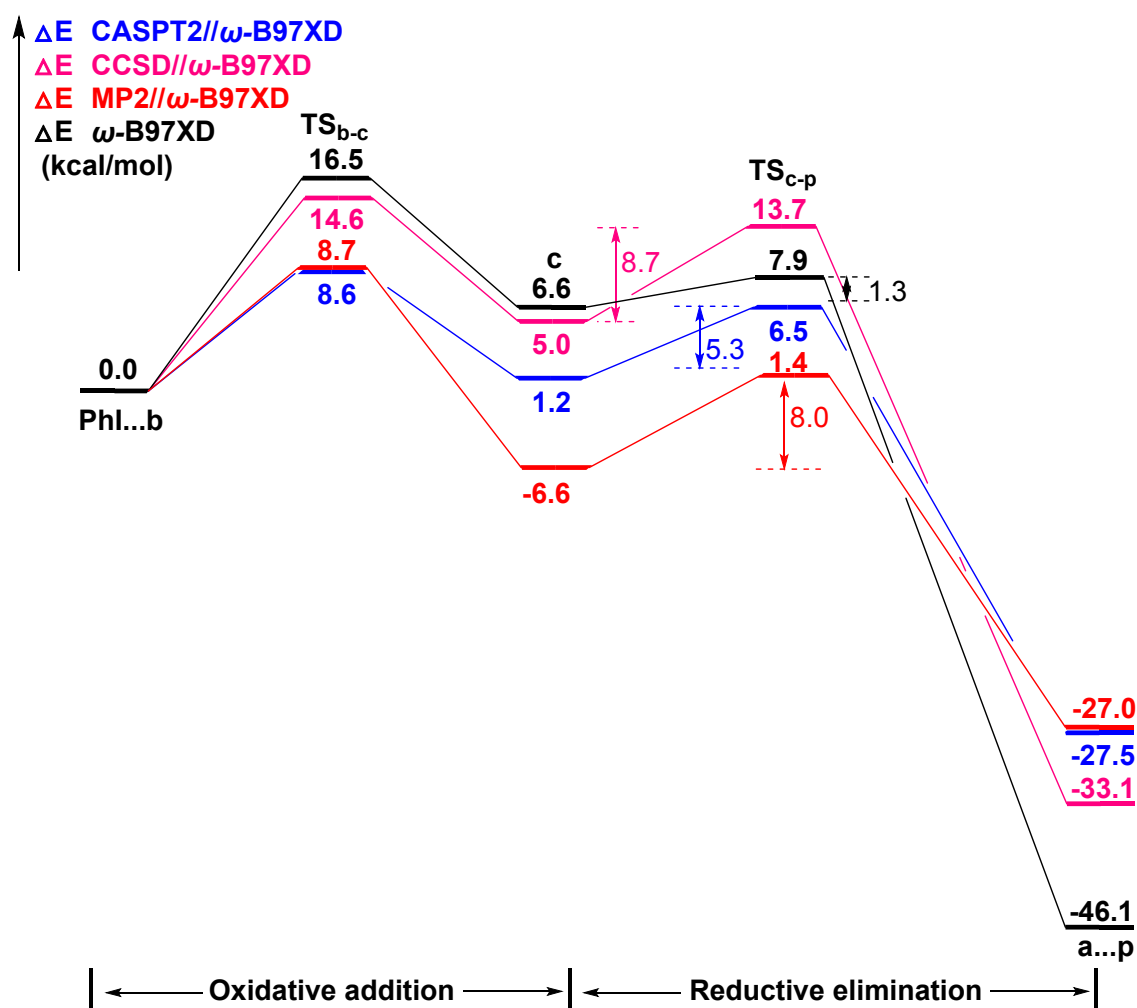
11

12   **Figure 5.** Electronic energy profile of OA-RE mechanism calculated by ω-B97XD, MP2//ω-B97XD

13   CCSD//ω-B97XD and CASPT2//ω-B97XD levels of theory. To enable a direct comparison in activation

14   barrier of OA step between DFT and CASPT2 methods, we took the **PhI...b** energy as the reference

15   (energy zero).

16

17   **3.5 Analyses on geometry, energy, and electronic structure along the OA-RE pathway.**

18   **3.5.1 DFT and CASSCF/CASPT2 calculations in the OA step.**

1   In this section, we discuss the potential energy curves along the OA step to estimate the stationary

2   and transition-state geometries of the CASPT2 method based on intrinsic reaction coordinate (IRC)

3   calculations using the ω-B97XD functional. In the CASPT2 calculations of the OA step, we used the

4   same active space defined in TS_{b-c} for all points on the IRC (see Figure S6). The IRC profile obtained

5   by ω-B97XD calculation was qualitatively consistent with that evaluated by CASPT2//ω-B97XD

6   calculation (see Figure 6). However, the activation energy of the TS_{b-c} step calculated by the ω-B97XD

7   functional (18.2 kcal/mol) was obviously higher than that calculated by CASPT2 method (8.8 kcal/mol).

8   Therefore, the ω-B97XD functional somewhat overestimates the activation energy of the OA step.

9   Moreover, the energy maximum was found at -1.7 amu$^{1/2}$ bohr on the ω-B97XD-calculated IRC. Thus,

10   the CASPT2 transition state is slightly closer to the **PhI...b** geometry than the ω-B97XD-calculated

11   transition state TS_{b-c}. Note that the CASPT2 energy at 0.0 amu$^{1/2}$ bohr (the ω-B97XD-optimised TS_{b-c})

12   was 1.1 kcal/mol lower than the energy maximum, indicating that the $\Delta E_{CASPT2//\omega\text{-}B97XD}$ even slightly

13   underestimated the activation energy of the OA step.
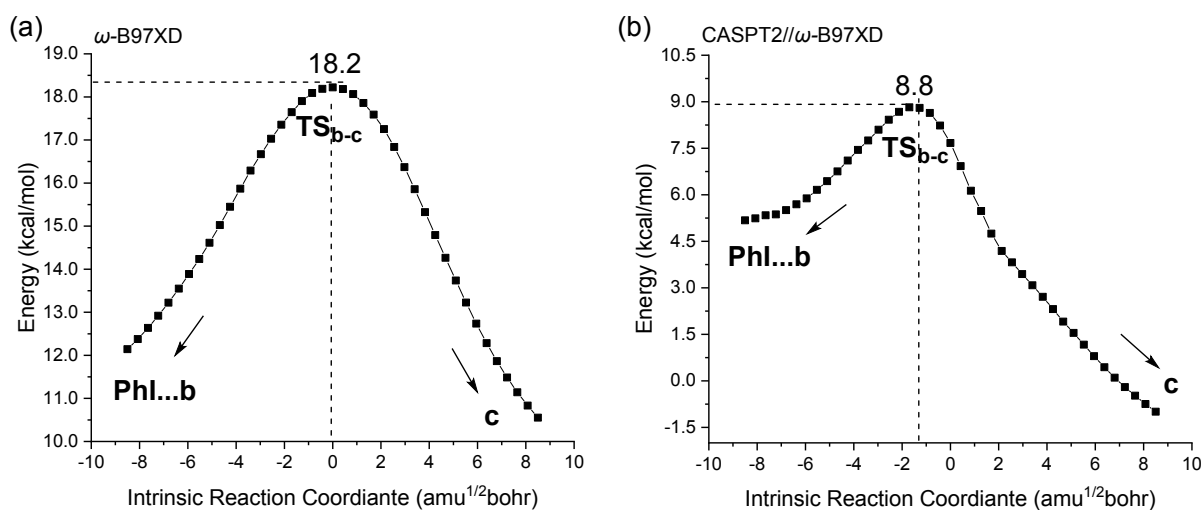
15 **Figure 6.** (a) the IRC of TS_{b-c} calculated by ω-B97XD in OA step; (b) the IRC of TS_{b-c} calculated by

16 CASSCF/CASPT2 in OA.

17

18   To discuss the changes in the electronic structure during the reaction, we plotted the sums of the d-

19 electron populations (q_{sum}) calculated by the DFT and CASSCF methods (Figure 7), where natural

20 population analysis (NPA) was employed in the DFT calculations and Mulliken population analysis was

21 employed in the CASSCF calculations. As shown in Figure 7, the q_{sum} by DFT decreases from 9.88 to

22 9.47 and the q_{sum} by CASSCF decreases from 9.90 to 9.46 during the OA step, suggesting that the

23 electronic densities of DFT and CASSCF are consistent with each other.

24
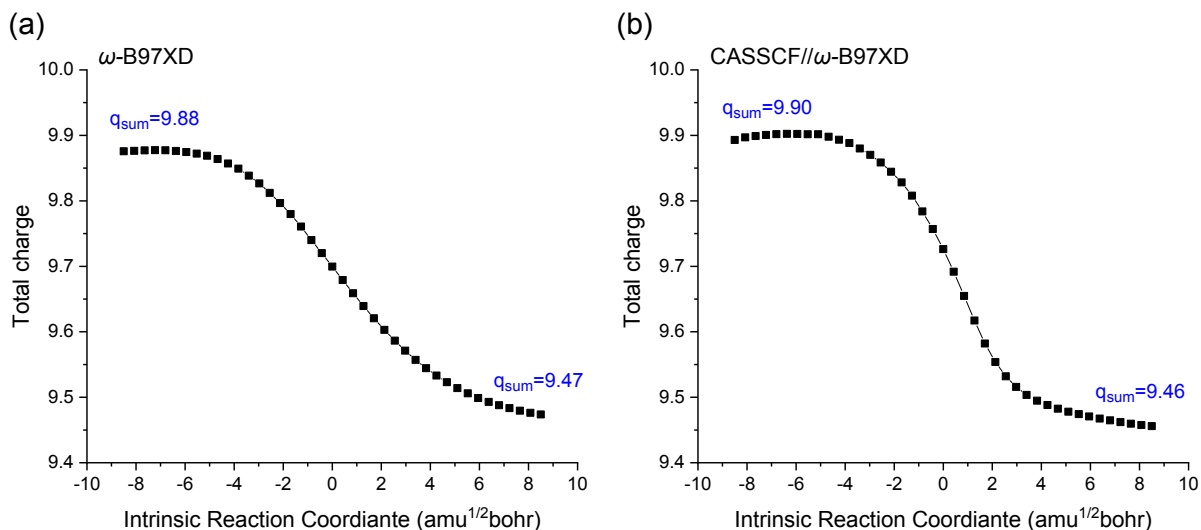
Figure 7. (a) the total charge of 3d orbitals along with IRC of **TS$_{b-c}$** calculated by ω-B97XD method in OA step; (b) the total charge of 3d orbitals along with IRC of **TS$_{b-c}$** calculated by CASSCF//ω-B97XD method in OA step.

To characterise the changes in the electronic structure in detail, we focused on two important natural orbitals (NOs) from the CASSCF wavefunction, which showed remarkable changes in occupation numbers during the OA step, as shown in Figure 8. Notably, the occupation number of the occupied 3dπ orbital decreases from 1.98 to 1.86, while the occupation number of the corresponding unoccupied 3dπ' orbital increases from 0.02 to 0.14, toward the OA reaction. As shown in the orbital picture, the 3dπ orbital interacts with the C-I antibonding σ* orbital to form Cu-C and Cu-I bonds, leading to the formation of Cu(III) species. At the end of the OA step, the occupation number of the 3dπ orbital is 1.86, which is significantly different from 2 (doubly occupied), and that of the 3dπ' orbital is 0.14, which is significantly different from 0 (unoccupied). Thus, we concluded that there was a slightly larger static electron correlation effect on this Cu(III) species than the reactant complex, and the large energy difference between the DFT and CASPT2 methods could be understood as an insufficient description of the electron correlation effect in the DFT calculations for this Cu(III) species.

16

1
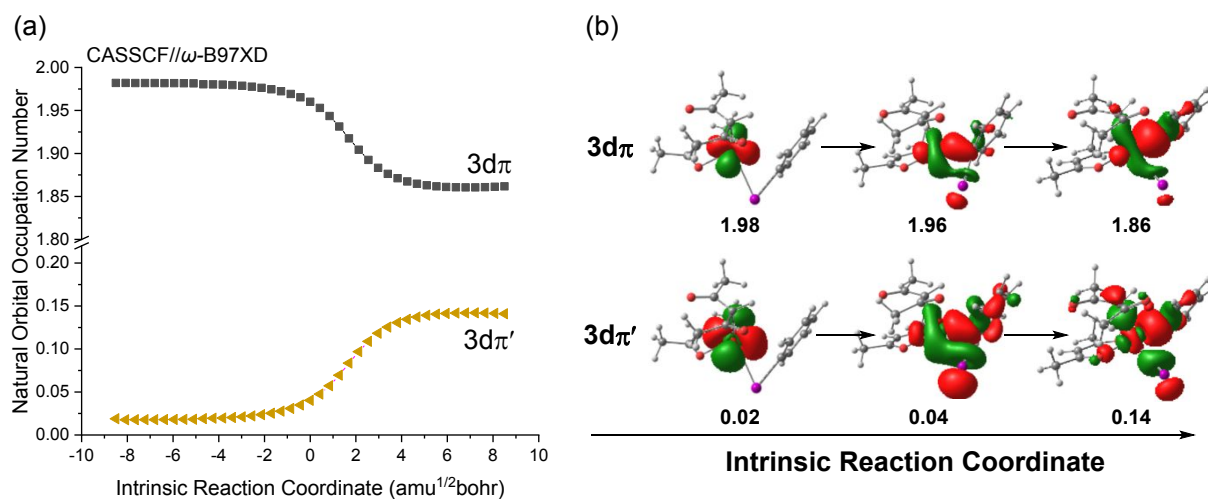
Figure 8. The occupation number of the important 3d orbital along with IRC of **TS$_{b-c}$** calculated by CASSCF//ω-B97XD in OA step.

3.5.2 DFT and CASSCF/CASPT2 calculations in the RE step.

Next, we discuss the potential energy curves along the RE step to estimate the transition state geometry of the CASPT2 method based on IRC calculations using the ω-B97XD functional. In the CASPT2 calculations of the RE step, we used the same active space defined in **TS$_{c-p}$** for all points on the IRC (see Supporting Information for details). The IRC profile obtained by ω-B97XD calculation agreed qualitatively with that evaluated by the CASPT2//ω-B97XD calculation (see Figure 9). The activation barriers measured from intermediate **c** were 4.3 and 9.9 kcal/mol for ω-B97XD and CASPT2//ω-B97XD, respectively. Therefore, the ω-B97XD functional underestimates the activation energy of the RE step. Furthermore, the energy maximum was located at 1.3 amu$^{1/2}$ bohr on the ω-B97XD-calculated IRC. Hence, the CASPT2 transition state is slightly closer to the **a...p** geometry than the ω-B97XD-optimised transition state **TS$_{c-p}$** in the RE step. Note that the CASPT2 energy at 0.0 amu$^{1/2}$ bohr (the ω-B97XD-optimised **TS$_{c-p}$**) was 1.5 kcal/mol lower than the energy maximum, indicating that the $\Delta E_{CASPT2//\omega\text{-B97XD}}$ slightly underestimated the activation energy of the RE step, as similar to that of the OA step.
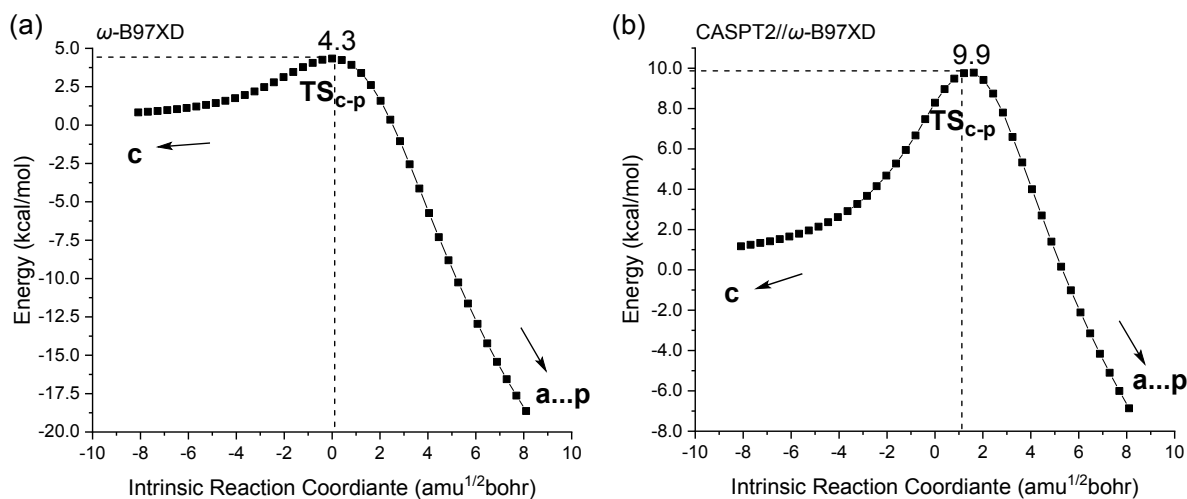
Figure 9. (a) the IRC of TS_{c-p} calculated by B3LYP-D3 in RE step; (b) IRC of TS_{c-p} calculated by CASSCF/CASPT2 in RE step.

We also plotted the sums of the d-electron populations (q_{sum}) calculated using the NPA charges from the DFT calculations and the Mulliken charges from the CASSCF calculations (Figure 10). In contrast to the OA step (Figure 7), the q_{sum} by DFT increases from 9.48 to 9.89, and the q_{sum} by CASSCF increases from 9.51 to 10.00 during the RE step. These results are consistent with the OA-RE mechanism and suggest that both DFT and CASSCF provide reliable electronic densities to explain the OA-RE steps.
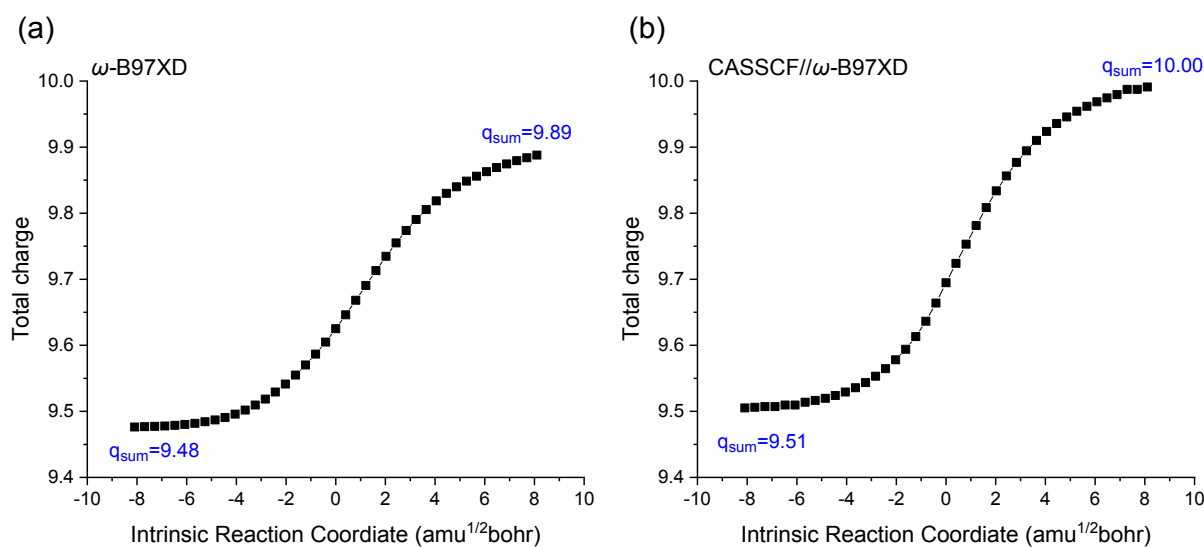

Figure 10. (a) the total charge of 3d orbitals along with IRC of TS_{c-p} calculated by ω-B97XD method in RE step; (b) the total charge of 3d orbitals along with IRC of TS_{c-p} calculated by CASSCF//ω-B97XD method in RE step.

The changes in the NOs and their occupation numbers for the RE step are summarised in Figure 11,

which are similar to those for the OA step (Figure 8). As a result of the Cu center reduction, the

occupation number of the 3dπ orbital increases from 1.89 to 1.98, while the occupation number of the

3dπ' orbital decreases from 0.14 to 0.02. Based on the orbital pictures, the 3dπ orbital interacts with the

Cu-C antibonding σ* orbital to form a new C-C covalent bond between the phenyl and methyl ligands,

resulting in the formation of the product complex. In the product complex, the occupation number of

the 3dπ orbital is almost 2 (doubly-occupied), while that of the 3dπ' orbital is almost 0 (unoccupied).

Thus, electron correlation effect in the product complex was not significant.
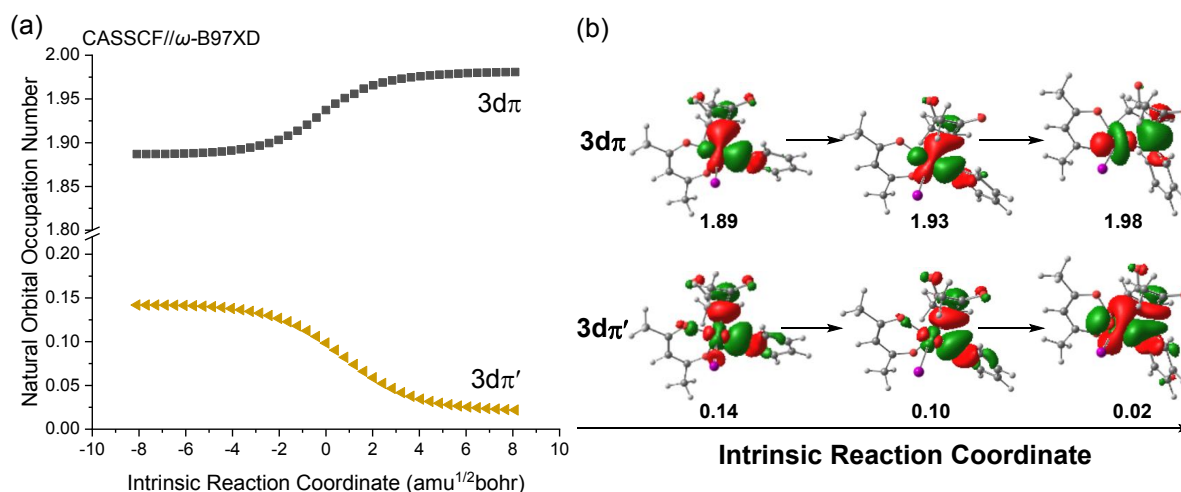
Figure 11. The occupation number of the important 3d orbital along with IRC of **TS$_{c-p}$** calculated by CASSCF//ω-B97XD in RE step.

4. Conclusions

In this study, the molecular mechanism of the Cu-catalysed coupling reaction between aryl iodides and β-diketones was studied theoretically based on density functional theory (DFT) and a multi-reference method (CASSCF/CASPT2). Based on the Cu(I) and Cu(II) active species, the reaction mechanisms OA-RE, IAT, SET, and σ-bond metathesis were investigated. Our DFT and CASSCF/CASPT2 calculations revealed that the catalytic cycle proceeds via OA and RE reactions, where the OA step is the rate-determining step. The functional dependencies of energy and geometry were assessed using the CASSCF/CASPT2 method. Interestingly, although the DFT-calculated activation energies were highly dependent on the choice of functionals, the CASSCF/CASPT2 results were less affected by the choice of DFT-optimised geometries. From our results, we concluded that the ω-B97XD-optimized geometry was closer to the CASSCF/CASPT2-optimized geometry. This arises from the shorter C-C bond distance between β-diketone and phenyl groups of the ω-B97XD-optimized **TS$_{c-p}$** than those of the other functionals. Although ω-B97XD functional would not always be an optimal choice for other systems, the DFT-optimized geometry is of good qualitative use for energetics at the CASPT2 level of theory after careful assessments. In the OA step, the natural orbitals from the CASSCF calculations describe the interaction between the 3dπ orbital and the C-I antibonding σ* orbital, which forms the coordination bonds of Cu-C and Cu-I, resulting in Cu(III) species. In the RE step, the natural

orbitals from the CASSCF calculation describe the interaction between the 3dπ orbital and the Cu-C antibonding σ^* orbital, which leads to a new C-C covalent bond between the phenyl and methyl ligands to afford the product complex.

The energy profiles and IRC curves obtained using the ω-B97XD functional and CASSCF/CASPT2 methods are compared. Interestingly, these were consistent with each other, at least qualitatively, suggesting that the ω-B97XD functional would be useful for investigating Cu complexes after reasonable assessment using the CASSCF/CASPT2 method. Based on population analyses along the reaction coordinates, the ω-B97XD-calculated electronic structure was also consistent with the CASSCF-calculated structure in both the OA and RE steps. The natural orbital occupation numbers of the CASSCF calculations showed that the ground state is almost single-reference in the course of reactions. However, slightly smaller occupation numbers of 3dπ orbitals in complex **c** indicated that the strong electron correlation effects were observed with the formation of the Cu(III) species; thus, DFT does not work for quantitative energy calculations around the Cu(III) intermediate complex.

Our results provide a better understanding of the mechanisms of Cu-catalysed coupling reactions from the perspective of the 3d electron correction effect of the Cu centre. It was also shown that the DFT-optimised geometry is sometimes very useful, even though the energy is not accurate. Finally, we provide valuable theoretical guidance for DFT/CASPT2-hybrid computational studies.

Acknowledgements

1   **References**

2   1.   P. Hohenberg and W. Kohn, *Phys. Rev.* , 1964, **136**, B864-B871.

3   2.   I. Obot, D. Macdonald and Z. Gasem, *Corros. Sci.*, 2015, **99**, 1-30.

4   3.   J. M. Seminario, 1996.

5   4.   W. Koch and M. Holthausen, VCH, Weinheim, Germany2001.

6   5.   K. D. Vogiatzis, M. V. Polynski, J. K. Kirkland, J. Townsend, A. Hashemi, C. Liu and
7   E. A. Pidko, *Chem. Rev.*, 2019, **119**, 2453-2523.

8   6.   M. G. Delcey, K. Pierloot, Q. M. Phung, S. Vancoillie, R. Lindh and U. Ryde, *PCCP*,
9   2014, **16**, 7927-7938.

10   7.   M. Kaupp, R. Reviakine, O. L. Malkina, A. Arbuznikov, B. Schimmelpfennig and V.
11   G. Malkin, *J. Comput. Chem.*, 2002, **23**, 794-803.

12   8.   M. C. Holthausen, *J. Comput. Chem.*, 2005, **26**, 1505-1518.

13   9.   B. O. Roos, P. R. Taylor and P. E. M. Sigbahn, *Chem. Phys.*, 1980, **48**, 157-173.

14   10.   B. O. Roos, *Adv. Chem. Phys.*, 1987, **69**, 399.

15   11.   K. Andersson, P. A. Malmqvist, B. O. Roos, A. J. Sadlej and K. Wolinski, *J. Phys.*
16   *Chem.*, 1990, **94**, 5483-5488.

17   12.   K. Andersson, P. Å. Malmqvist and B. O. Roos, *J. Chem. Phys.*, 1992, **96**, 1218-1226.

18   13.   P. Pulay, *Int. J. Quantum Chem*, 2011, **111**, 3273-3279.

19   14.   Y. Yang, J. Liang, W. Li, W. Yang, C. Wang, X. Zhang, W.-H. Fang, Z. Guo and X.
20   Chen, *J. Phys. Chem. A*, 2023, **127**, 4115-4124.

21   15.   D. Vrška, P. Neogrády, V. Kellö, M. Urban and M. Pitoňák, *Int. J. Quantum Chem*,
22   2023, e27122.

23   16.   D. Vörös and S. Mai, *J. Comput. Chem.*, 2023, **44**, 1381-1394.

24   17.   B. Kintzel, M. Böhme, D. Plaul, H. Görls, N. Yeche, F. Seewald, H.-H. Klauss, A. A.
25   Zvyagin, E. Kampert, T. Herrmannsdörfer, G. Pascua, C. Baines, H. Luetkens and W.
26   Plass, *Inorg. Chem.*, 2023, **62**, 3420-3430.

27   18.   J. Soto, D. Peláez and M. Algarra, *J. Chem. Phys.*, 2023, **158**, 204301.

28   19.   S. Sader and E. Miliordos, *J. Phys. Chem. A*, 2021, **125**, 2364-2373.

29   20.   S. N. Khan and E. Miliordos, *J. Phys. Chem. A*, 2019, **123**, 5590-5599.

30   21.   M. Feldt, C. Martín-Fernández and J. N. Harvey, *PCCP*, 2020, **22**, 23908-23919.

31   22.   R. Han and S. Luber, *J. Comput. Chem.*, 2020, **41**, 1586-1597.

32   23.   C. Liu, H. Zhang, W. Shi and A. Lei, *Chem. Rev.*, 2011, **111**, 1780-1824.

33   24.   B. A. Baviskar, P. V. Ajmire, D. S. Chumbhale, M. S. Khan, V. G. Kuchake, M.
34   Singupuram and P. R. Laddha, *Sustain Chem Pharm*, 2023, **32**, 100953.

35   25.   L. Zheng, X. Guo, Y. C. Li, Y. Wu, X. S. Xue and P. Wang, *Angew. Chem. Int. Ed.*,
36   2023, **62**, e202216373.

37   26.   R. Jana, T. P. Pathak and M. S. Sigman, *Chem. Rev.*, 2011, **111**, 1417-1492.

38   27.   P. M. MacQueen, J. P. Tassone, C. Diaz and M. Stradiotto, *J. Am. Chem. Soc.*, 2018,

140, 5023-5027.

28. J. A. Terrett, J. D. Cuthbertson, V. W. Shurtleff and D. W. MacMillan, *Nature*, 2015, **524**, 330-334.

29. F. Ullmann and J. Bielecki, *Ber. Dtsch. Chem. Ges.*, 1901, **34**, 2174-2185.

30. H.-P. Bi, L. Zhao, Y.-M. Liang and C.-J. Li, *Angew. Chem. Int. Ed.*, 2009, **48**, 792-795.

31. F. Ullmann, *Ber. Dtsch. Chem. Ges.*, 1904, **37**, 853-854.

32. F. Ullmann and P. Sponagel, *Justus. Liebigs. Ann. Chem.*, 1906, **350**, 83-107.

33. A. Ouali, J. F. Spindler, H. J. Cristau and M. Taillefer, *Adv. Synth. Catal.*, 2006, **348**, 499-505.

34. G. Nordmann and S. L. Buchwald, *J. Am. Chem. Soc.*, 2003, **125**, 4978-4979.

35. D. Ma and Q. Cai, *Org. Lett.*, 2003, **5**, 3799-3802.

36. F. Ullmann, *Ber. Dtsch. Chem. Ges.*, 1903, **36**, 2382-2384.

37. K. Kunz, U. Scholz and D. Ganzer, *Synlett*, 2003, **2003**, 2428-2439.

38. G. Evano, N. Blanchard and M. Toumi, *Chem. Rev.*, 2008, **108**, 3054-3131.

39. E. Sperotto, G. P. M. van Klink, G. van Koten and J. G. de Vries, *Dalton. Trans.*, 2010, **39**, 10338-10351.

40. C. Sambiagio, S. P. Marsden, A. J. Blacker and P. C. McGowan, *Chem. Soc. Rev.*, 2014, **43**, 3525-3550.

41. G. O. Jones, P. Liu, K. N. Houk and S. L. Buchwald, *J. Am. Chem. Soc.*, 2010, **132**, 6205-6213.

42. H.-Z. Yu, Y.-Y. Jiang, Y. Fu and L. Liu, *J. Am. Chem. Soc.*, 2010, **132**, 18078-18091.

43. Y. Liu, A. Feng, R. Zhu, C. Liu and D. Zhang, *J. Catal.*, 2023.

44. R. G. R. Bacon and O. J. Stewart, *J. Chem. Soc.*, 1965, 4953-4961.

45. K. Mullick, S. Biswas, C. Kim, R. Ramprasad, A. M. Angeles-Boza and S. L. Suib, *Inorg. Chem.*, 2017, **56**, 10290-10297.

46. C. Zhang, C. Tang and N. Jiao, *Chem. Soc. Rev.*, 2012, **41**, 3464-3484.

47. G. Lefèvre, A. Tlili, M. Taillefer, C. Adamo, I. Ciofini and A. Jutand, *Dalton. Trans.*, 2013, **42**, 5348-5354.

48. J.-M. Li, Y.-H. Wang, Y. Yu, R.-B. Wu, J. Weng and G. Lu, *ACS Catalysis*, 2017, **7**, 2661-2667.

49. A. M. Suess, M. Z. Ertem, C. J. Cramer and S. S. Stahl, *J. Am. Chem. Soc.*, 2013, **135**, 9797-9804.

50. C. He, G. Zhang, J. Ke, H. Zhang, J. T. Miller, A. J. Kropf and A. Lei, *J. Am. Chem. Soc.*, 2013, **135**, 488-493.

51. K. Pierloot, in *Computational Organometallic Chemistry*, ed. T. R. Cundari, Marcel Dekker, Inc., New York, 2001, pp. 123-158.

52. S. Vancoillie and K. Pierloot, *J. Phys. Chem. A*, 2008, **112**, 4011-4019.

53. M. Flock and K. Pierloot, *J. Phys. Chem. A*, 1999, **103**, 95-102.

54. K. Pierloot, J. O. A. De Kerpel, U. Ryde, M. H. M. Olsson and B. O. Roos, *J. Am. Chem. Soc.*, 1998, **120**, 13156-13166.

55. B. Vlaisavljevich and T. Shiozaki, *J. Chem. Theory Comput.*, 2016, **12**, 3781-3787.

56. G. F. S. Fernandes, M. A. P. Pontes, F. B. C. Machado and L. F. A. Ferrão, *Comput. Theor. Chem.*, 2022, **1207**, 113502.

57. M. J. Frisch, G. W. Trucks, H. B. Schlegel, G. E. Scuseria, M. A. Robb, J. R. Cheeseman, G. Scalmani, V. Barone, G. A. Petersson, H. Nakatsuji, X. Li, M. Caricato, A. V. Marenich, J. Bloino, B. G. Janesko, R. Gomperts, B. Mennucci, H. P. Hratchian, J. V. Ortiz, A. F. Izmaylov, J. L. Sonnenberg, D. Williams-Young, F. Ding, F. Lipparini, F. Egidi, J. Goings, B. Peng, A. Petrone, T. Henderson, D. Ranasinghe, V. G. Zakrzewski, J. Gao, Rega, N., G. Zheng, W. Liang, M. Hada, M. Ehara, K. Toyota, R. Fukuda, J. Hasegawa, M. Ishida, T. Nakajima, Y. Honda, O. Kitao, H. Nakai, T. Vreven, K. Throssell, M. Jr., P. J.A., J.E., F. Ogliaro, M. J. Bearpark, J. J. Heyd, E. N. Brothers, K. N. Kudin, V. N. Staroverov, T. A. Keith, R. Kobayashi, J. Normand, K. Raghavachari, A. P. Rendell, J. C. Burant, S. S. Iyengar, J. Tomasi, M. Cossi, J. M. Millam, M. Klene, C. Adamo, R. Cammi, J. W. Ochterski, R. L. Martin, K. Morokuma, O. Farkas, J. B. Foresman and D. J. Fox, Gaussian 16 Revision. B.01, Gaussian, Inc., Wallingford CT, 2016.

58. M. Dolg, U. Wedig, H. Stoll and H. Preuss, *J. Chem. Phys.*, 1987, **86**, 866-872.

59. A. Bergner, M. Dolg, W. Küchle, H. Stoll and H. Preuß, *Mol. Phys.*, 1993, **80**, 1431-1441.

60. J. Tomasi, B. Mennucci and R. Cammi, *Chem. Rev.*, 2005, **105**, 2999-3094.

61. F. Aquilante, J. Autschbach, R. K. Carlson, L. F. Chibotaru, M. G. Delcey, L. De Vico, I. Fdez. Galván, N. Ferré, L. M. Frutos, L. Gagliardi, M. Garavelli, A. Giussani, C. E. Hoyer, G. Li Manni, H. Lischka, D. Ma, P. Å. Malmqvist, T. Müller, A. Nenov, M. Olivucci, T. B. Pedersen, D. Peng, F. Plasser, B. Pritchard, M. Reiher, I. Rivalta, I. Schapiro, J. Segarra-Martí, M. Stenrup, D. G. Truhlar, L. Ungur, A. Valentini, S. Vancoillie, V. Veryazov, V. P. Vysotskiy, O. Weingart, F. Zapata and R. Lindh, *J. Comput. Chem.*, 2016, **37**, 506-541.

62. V. Veryazov, P.-O. Widmark, L. Serrano-Andrés, R. Lindh and B. O. Roos, *Int. J. Quantum Chem*, 2004, **100**, 626-635.

63. N. Forsberg and P.-Å. Malmqvist, *Chem. Phys. Lett.*, 1997, **274**, 196-204.